Materials Science & Engineering A 688 (2017) 169–173

Contents lists available at ScienceDirect

Materials Science & Engineering A

journal homepage: www.elsevier.com/locate/msea

Reversible twin boundary migration between α″ martensites in a Ti-Nb-Zr-Sn alloy

Tingting Yao, Kui Du*, Haoliang Wang, Lu Qi, Suyun He, Yulin Hao, Rui Yang, Hengqiang Ye

Shenyang National Laboratory for Materials Science, Institute of Metal Research, Chinese Academy of Sciences, Shenyang 110016, People's Republic of China

ARTICLE INFO

Keywords:
Grain boundaries
Microanalysis
Martensitic transformations
Titanium alloys

ABSTRACT

Cyclic tensile loading tests and transmission electron microscopy investigation are conducted on a Ti-24Nb-4Zr-8Sn (wt%) alloy. Under tensile strain less than 3.3%, most of the deformation strain recovers after unloading but significant energy dissipation occurs during the loading-unloading cycle. Reversible migration of twin boundaries between α″ martensite variants, in virtue of dislocation movement on the twin boundaries, has been revealed by time resolved high-resolution transmission electron microscopy. This twin boundary migration contributes to the energy dissipation effect and consequently the damping property of the titanium alloy.

1. Introduction

In the past decades there has been increasing interest in developing high damping materials for technological applications [1,2]. A number of high damping materials have been designed which combine superior damping property with good strength, such as Ti-Ni-based alloys and Cu-Zn alloys [3–5]. For most of these alloys, phase transformation is one of effective mechanisms of high damping property [6], those include temperature induced and stress induced phase transformations [7,8]. The temperature induced martensitic transformation is a major origin of the damping property in shape memory alloys, which are typical high damping materials [9,10]. Meanwhile, the hysteretic movement of interfaces can also cause energy dissipation [11–13].

Ti-24Nb-4Zr-8Sn (wt%) (Ti2448) alloy is a new β-type titanium alloy, which exhibits a superelasticity of about 3.3% and a superior damping capacity after solution treatment and flash treatment [14–16]. Recently, researches have conducted to understand origins of shape memory and superelasticity effects in β-type titanium alloys, primarily the thermoelastic cycling phase transformation from β phase (body centered cubic) to α″ phase (*c*-centered orthorhombic) or α phase (hexagonal close-packed) between high temperature and low temperature [17–20].

The objective of this paper is to correlate cyclic tensile test properties with deformation-induced microstructure changes in Ti2448 alloy. The energy dissipation corresponding to the change of microstructures is discussed based on time resolved high-resolution transmission electron microscopy (HRTEM) investigation.

2. Materials and methods

An alloy ingot was prepared with the composition of Ti-24Nb-4Zr-8Sn (wt%) by vacuum arc melting using Ti-Sn master alloy and pure Ti, Nb and Zr. The ingot was then hot forged at 1273 and 1123 K into bars of 25 mm in diameter. Cylinders with the diameter of 8.6 mm were cut from the as-forged bars and used for crystal growth. Single crystals of 9 mm in diameter and 50 mm in length were grown by an optical floating-zone furnace (FZ-T-12000-X-VP-S, Crystal System Inc.). The growth direction is parallel to the $<110>_{\beta}$ crystallographic orientation within 1° deviation, which was verified by the Laue X-ray back reflection technique. The detailed procedures have been described in previous study [21].

Tensile specimens of 3 mm in diameter and 20 mm in parallel length were machined along the longitudinal direction of the single crystal rods. The surface of specimens has been polished prior to tensile measurements. Cyclic loading-unloading test was conducted at room temperature (~21 °C) with a constant strain rate of 2.5×10^{-4} s^{-1} on an Instron 5582 universal test machine. The stress-strain curves were recorded by an Instron 2620-601 extensometer. Fourteen loading-unloading cycles were conducted with no pause during the entire cyclic loading-unloading test. Interrupted tensile tests were also performed for microstructure investigation at different deformation stages.

Transmission electron microscopy (TEM) and in-situ TEM were used to identify the microstructure evolution under tensile loading. TEM samples were prepared using twin-jet electro-polishing (Tenupol-5 machine) and finished with low voltage Ar ion milling (Gatan 691 Precision Ion Polishing System with liquid nitrogen cooling). The electrolyte comprised of 6% $HClO_4$, 59% CH_3OH and 35%

* Corresponding author.
E-mail address: kuidu@imr.ac.cn (K. Du).

http://dx.doi.org/10.1016/j.msea.2017.02.001
Received 27 December 2016; Received in revised form 1 February 2017; Accepted 1 February 2017
Available online 02 February 2017

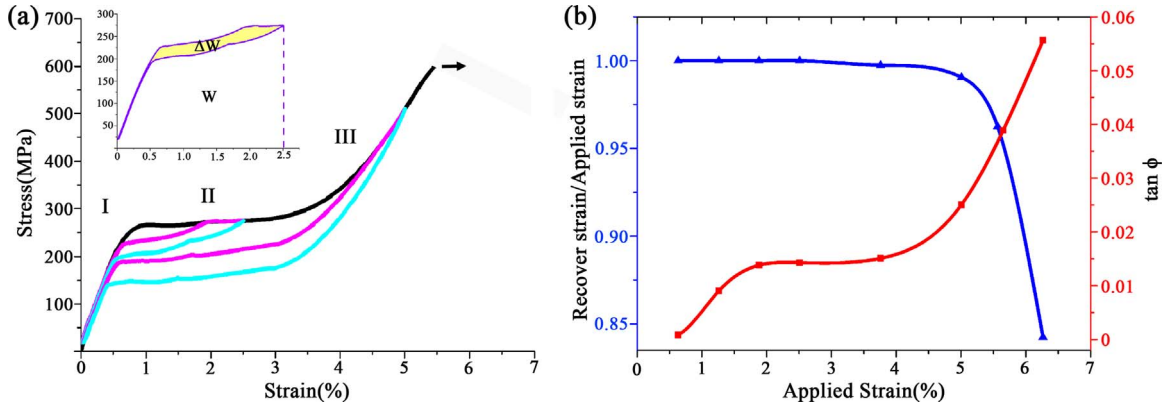

Fig. 1. (a) The stress-strain curve of a Ti2448 single crystal sample under tension along the $[110]_\beta$ axis (black), and stress-strain curves of tensile loading (purple) and unloading (blue). Inset shows an illustration for the determination of energy dissipation ($\Delta W/2\pi W$). ΔW is the area of the stress-strain loops, W is the area of stress-strain under loading in the same cycle. (b) The relationship of the ratio of recovered strain to applied strain versus the applied strain (dark blue), and tan ϕ versus the applied strain curve (red). (For interpretation of the references to color in this figure legend, the reader is referred to the web version of this article.)

$CH_3(CH_2)_3OH$ in volume percent. With tensile loading-unloading, time resolved HRTEM images were recorded at 10 frames per second on single crystal specimens in an FEI Tecnai F20 TEM at room temperature. The tension was on the $[110]_\beta$ direction approximately, applied by a Gatan Model 654 single-tilt straining holder at a speed of 0.1 μm/s.

3. Results and discussion

On account of different mechanical characteristics of the stress-strain relationship (Fig. 1a), the curve can be divided into three stages, termed as stages I, II and III here. They correspond to a linear response prior to a stress plateau, the stress plateau of approximately 270 MPa and the subsequent strain hardening stage, respectively. The ratio of recovered strain to applied strain is calculated based on the tensile test data, and the ratio versus the applied strain is drawn in Fig. 1b. It shows that the applied strain can be almost fully recovered until the applied strain reaches 3.3%. Beyond that, the ratio decreases with the increasing applied strain significantly.

The energy dissipation is estimated for cyclic loading processes, which is also expressed as the energy loss factor (tan ϕ) for different applied strain: tan ϕ =$\Delta W/2\pi W$. In this equation, ΔW is the energy dissipated in a full cycle, W is the maximum stored energy [22]. At the initial deformation stage, where the applied strain is less than 1.8%, the value of tan ϕ is low and increases slightly with the applied strain. With higher applied strain, the tan ϕ keeps constant under the strain between 1.8% and 3.3%, which fits the strain range of the stage II in the tensile stress-strain curve. Subsequently, after the applied strain higher than 3.3%, which means deformation enters the stage III, the value of tan ϕ increases significantly. The inflection points of the tan ϕ versus applied strain curve (Fig. 1b) are almost the same as that in the stress-strain curve (Fig. 1a).

Microstructure investigations are conducted on the TEM samples corresponding to different deformation stages, which are obtained from interrupted and fractured tensile tests, and presented in Fig. 2 and Fig. 3. Sample S1 is chosen with a terminal stress at the stress plateau, while sample S2 is prepared from a fractured specimen. These indicate that the deformation in S1 corresponds to the stress plateau (stage II), and S2 to the strain hardening stage (stage III).

The selected area electron diffraction (SAED) image in Fig. 2a confirms that α″ plates are in twin relationship, which is obtained from deformation induced α″ plates in sample S1. According to dark-field TEM images (Fig. 2b–c), these α″ plates almost align in one direction with a width range from 10 nm to 80 nm. Moreover, α″ plates are also observed in sample S2, however, they are often aligning in two directions, and intersect with each other (Fig. 3a). Even for the occasionally observed single directional α″ plates in sample S2 (Fig. 3b), they are much wider (with a mean width of approximately 100 nm) than α″ plates in sample S1. It is worth noting that nanometer-scaled α″ grains (Fig. 3c) are observed at this stage.

To verify and analyze the orientation relationship between the deformation induced α″ lamellae, Nanomegas TEM orientation imaging technique [23,24] is employed to obtain orientation maps of the specimen. This precession-assisted crystal orientation imaging technique can achieve orientation maps with a spatial resolution of approximately 2 nm [23,24].

The orientation maps obtained from the Ti2448 specimen is shown in Fig. 4. The phase image (Fig. 4c) shows the existence of β (white in Fig. 4c) and α″ phases (red) in the specimen. The orientation image further identifies two kinds of α″ lamellae with different orientations, presented in yellow and green in Fig. 4a. The Euler angles between α″ lamellae (yellow in Fig. 4a) and α''_T lamellae (green) have been calculated as 70.1 ± 2.6°. This confirms the twin relationship between the two kinds of α″ lamellae, which are considered as different variants of α″ martensite.

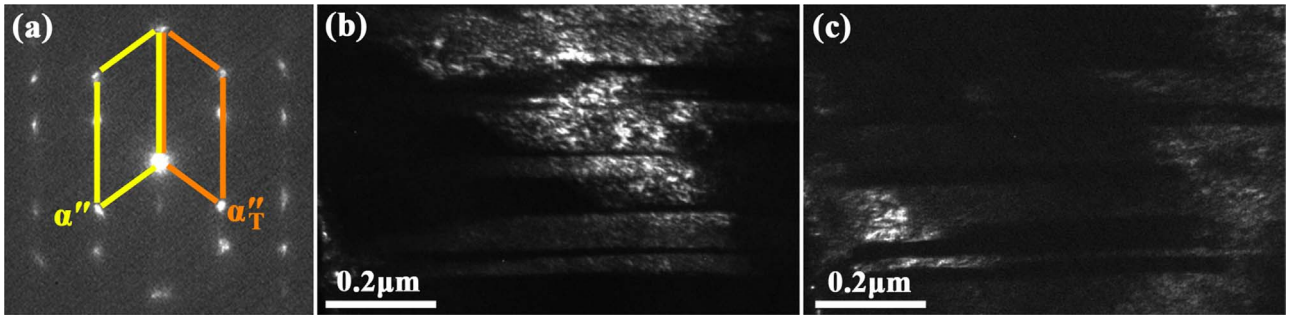

Fig. 2. Transmission electron microscopy (TEM) images of α″ martensites in interrupted tensile deformed specimen S1. (a) Selected area electron diffraction (SAED) image of α″ martensite plates aligning along one direction, presenting the twin relationship. (b–c) Dark-field images of α″ martensite plates.